Jurnal Teknologi

A Numerical Study of Heat Transfer to Turbulent Separation Nanofluid Flow in an Annular Passage
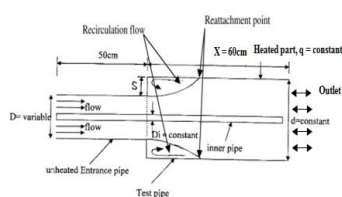
Omer A. Alawi, Nor Azwadi Che Sidik*, Wah Yen Tey

Faculty of Mechanical Engineering, Universiti Teknologi Malaysia, 81310 UTM Johor Bahru, Johor, Malaysia

*Corresponding author
azwadi@fkm.utm.my

Graphical abstract

Abstract

The separation and the reattachment of nanofluid flow through a sudden expansion in an annular passage have been studied. ANSYS FLUENT was deployed to simulate the effect of separation of nanofluid flow on the local and average convection heat transfer in an annular passage. The outer tube was made of aluminium with internal diameter of 83 mm and horizontal length of 600 mm, subjected to a constant wall heat flux. The investigation was performed with varying Reynolds number ranging from 5000 to 25000, heat flux from 719 W/m^2 to 2098 W/m^2, and the enhancement of step heights expanding from 0 mm (d/D=1) to 18.5 mm (d/D=1.8). The increase of flow velocity results in the sudden drop of the surface temperature in proximity to the pipe entrance, followed by gradual increment of surface temperature along the pipe. The minimum surface temperature could be obtained at flow reattachment point. The position of the minimum temperature point is independent on the inlet flow velocity. In general, the average Nusselt number increases with the increase of Reynolds number.

Keywords: Numerical simulation, concentric annular passage, heat exchanger, nanofluid

1.0 INTRODUCTION

Turbulent flow separation is an omnipresent natural phenomenon, formed when pressure gradient transpires as a result of alteration of geometries and boundary conditions. Such separations along with recirculation flows will give rise to pressure losses and intensification of turbulence, mass and heat transfer rates. Despite the lack of knowledge in the separation of fluid flow, it is applied in wide-ranging engineering industries and fluid machineries [1, 2]. When the fluid flows away from a finite boundary surface, then flow divergence and separation is developed [3]. The separation of fluid flow is well demonstrated in viscous flow. This can be ascribed to the fact that viscosity induces boundary layer separation, which is an instance of flow separation.

Flow separation, recirculation and reattachment can be easily formed during backward facing step flow, and its fundamental physics was explained by Togun *et al.* [4] and Wang *et al.* [5]. The parameters which impact on the separation process were studied, in the light of the engineering needs to make the process under control. Terekhov and Pahomov [6] and Kurtbas [7] had further conducted the general study on separation flow as well by observing and analysing the effects on flow field subjected to different Reynolds numbers.

Specifically in annular passage, Kays and Leung [8] have studied the convective heat transfer in a concentric circular tube when either the inner tube or outer tube was heated with a constant heat flux. They developed numerical solution (Fundamental Solutions of the Second Kind) to determine the relationship between Reynolds number and Nusselt number. Their findings with different radius ratio, Reynolds numbers and Prandtl numbers, were validated experimentally.

Barbosa et al [9] studied flow through annular ducts with pin fins in a double-pipe heat exchanger. 560 pins were attached to the annular inner wall with air flowing in. They presented their results in dimensionless form and computed the average Nusselt numbers and

friction factors as a function of the Reynolds number. They compared those findings with the case in which those fins were removed. The results of their work were used in present study for comparison purposes.
Filetti and Kays [10] conducted experiments to determine the local heat transfer rates of air flow near the entrance to a flat duct. Abrupt air flow cross sectional area enlargement can be observed with the enlargement area ratios (ratio of fluid flow cross sectional area after aperture to fluid flow cross sectional area before aperture) of 2.125 and 3.1, with Reynolds number based on the duct hydraulic diameter expanding from 70,000 to 205,000. This flow was characterized by a long stall on one side and a short stall on the other. For both cases, maximum heat transfer can be observed at reattachment point, followed by decreasing trend upon the formation of fully developed flow. It was found that boundary layer reattachment occurred at different distances in the upper and lower walls of the duct and these distances are independent of Reynolds numbers. In all the separation, reattachment and redevelopment region, the Nusselt number along downstream of the inner tube of annular passage exhibit the similar behavior. Davletshin *et al.* [11] considered a pulsating, superimposing free stream in his experimental study of heat transfer of turbulent separation flow field at the wake of an obstacle, and pronounced heat transfer intensification was found right in the separation region of the pulsating flow.

Numerical study on flow separation in a diverging conical duct is the theme of research reported by Sparraw *et al.* [12], investigating the effects of Reynolds number and divergence angle on the flow field along the duct. In their case, fully developed flow was assumed in the inlet of conical diffuser and the fluid was discharged to a long circular pipe. They used a universal flow-regime model for laminarization process of transitional and turbulent flow. The result showed that at the low Reynolds number regime (Re<2000), the flow separation appeared when the diffuser expanded with angle of 5°. This finding nullified a previous perception that separation happen with a divergence angle of 7°. Their experiments were run with the divergence angle spanning from 10° to 30°, and separation occurred at all the investigated Reynolds numbers. The relatively more elongated pattern of the separation was observed at the lower Reynolds numbers.

Cylindrical surface in annular passage is commonly used in industries namely turbine blade cooling, combustion chambers and duct connection. Despite sophisticated industrial design, an annulus space between two concentric-shape surfaces appears to be the simplest representation of such passage [13]. The advancement in computational techniques and instrumentations promote the investigations of fluid mechanics of complex three dimensional flow recirculation. The works were further extended to vertical, horizontal and inclined cases for different fluids, geometrical shapes and boundary conditions [14-17]. In a rectangular duct over inclined

backward-facing step, the convection flow was studied considering constant heat flux approach [18].

Chen *et al.* [19] studied a laminar conjugate heat transfer by natural convection and conduction with the heat source from an inner heat generating solid circular cylinder. Assumption was made such that the two sealed ends of the tube are adiabatic. Using the finite volume SIMPLE algorithm on the collocated arrangement, results were reported for temperature distributions and Nusselt numbers on different cross sectional planes and longitudinal sections, for Rayleigh number ranging from 10^5 to 10^8, solid volume fraction of $0 \leq \varphi \leq 0.05$ and different inclination angles.

Although most works have reported the flow reattachment on duct and circular pipe flow, the study on heat transfer and flow phenomena in annular passage retains room for further research. Such knowledge is notably critical for optimizing the performance in both the parallel and counter flow heat exchangers. Thus, the challenge of the current work is to collect new information on the influence of the turbulent flow on the recirculation region, especially on its spatial extension, comprising the heat transfer rate and the effect of flow separation due to sudden enlargement in the flow passage.

2.0 NUMERICAL PROCEDURE

2.1 Physical Model

The schematic drawing of the annular sudden expansion pipe flow is presented in Figure 1. The inner or outer surface temperature of the annular pipe with sudden expansion can be influenced by many parameters, such as flow velocity, surface heat flux, and the step heights. The fluid utilized to conduct heat transfer in this experiment is air. The inlet and outlet diameters of the pipe are 46 and 83 mm respectively and the inner tube diameter of the annular pipe is 22 mm. In the simulations, 2 different cases (d/D = 1 and 1.8) were considered over an annular passage. The surface heat flux of the annular pipe is selected within the range of 719 W/m^2 ≤ q ≤ 2098 W/m^2 with the variable Reynolds Number between 5000 to 25000. The numerical simulation parameters are summarized in Table 1.
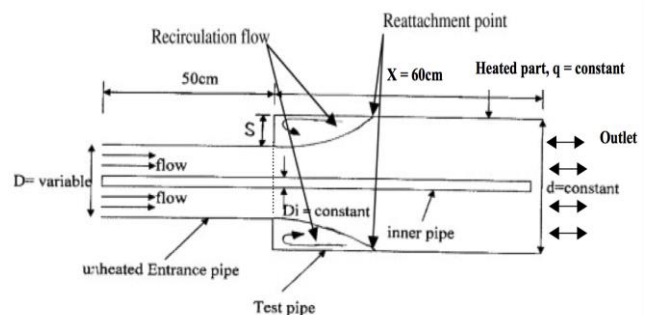
Figure 1 Schematic diagram of the annular sudden expansion in annular pipe flow

Table 1 Dimensions of the numerical model

Inner tube	Outer tube at entrance section	Outer tube at test section
D_i = 22 mm	d = 46 mm and 83 mm	D = 83 mm
L = 110 cm	L = 50 cm	L = 60 cm

2.2 Governing Equations

Fluid flow in a physical domain is governed by the laws of conservation of mass and momentum. These conservation laws, for steady flows in a two-dimensional domain can be stated by Equations. (1) to (6).

$$\frac{\partial u}{\partial x} + \frac{\partial v}{\partial y} = 0 \tag{1}$$

$$\rho \left(u \frac{\partial u}{\partial x} + v \frac{\partial u}{\partial y}\right) = -\frac{\partial p}{\partial x} + u \left(\frac{\partial^2 u}{\partial x^2} + \frac{\partial^2 u}{\partial y^2}\right) \tag{2} \rho \left(u \frac{\partial v}{\partial x} + v \frac{\partial v}{\partial y}\right)$$

$$= -\frac{\partial p}{\partial y} + u\left(\frac{\partial^2 v}{\partial x^2} + \frac{\partial^2 v}{\partial y^2}\right) \tag{2}$$

$$\rho \left(u \frac{\partial T}{\partial x} + v \frac{\partial T}{\partial y}\right) = \alpha \left(\frac{\partial^2 T}{\partial x^2} + \frac{\partial^2 T}{\partial y^2}\right) \tag{3}$$

$$\rho \left(u \frac{\partial T}{\partial x} + v \frac{\partial T}{\partial y}\right) = \alpha(\frac{\partial^2 T}{\partial x^2} + \frac{\partial^2 T}{\partial y^2}) \tag{4}$$

$$\frac{\partial}{\partial x}(\rho k \mu) = \frac{\partial}{\partial y}\left(\left[\left(\mu + \frac{\mu_t}{\sigma_k}\right) \frac{\partial k}{\partial y}\right]\right) + G_k - \rho_\varepsilon \tag{5}$$

$$\frac{\partial}{\partial x}(\rho \varepsilon \mu) = \frac{\partial}{\partial y}\left[\left(\mu + \frac{\mu_t}{\sigma_\varepsilon}\right) \frac{\partial \varepsilon}{\partial y}\right] + C_{1\varepsilon} \frac{\varepsilon}{k}(G_k + C_{3\varepsilon}G_b) - C_{2\varepsilon}\rho \frac{\varepsilon^2}{k} \tag{6}$$

σ_k and σ_ε are the turbulent Pr numbers for k and ε respectively, where by Pr can be defined as $\upsilon C_p/k$. The model constants are 1.44, 1.92, 0.09, 1.0 and 1.3 for $C_{1\varepsilon}$, $C_{2\varepsilon}$, C_μ, σ_k and σ_ε, respectively.

Flow solver was used to formulate mass, momentum and energy equations in partial differential form along with the two-dimensional Navier–Stokes equations. The finite volume method was selected to discretize Navier–Stokes equations with cells in the computational domain. With all above frameworks, the step in backward-facing cases is perpendicular to the stepped wall. In this geometry, there is sudden expansion or contraction in the flowing fluid passage. Numerical solution of the governing equations for turbulent flow was performed by using SIMPLE Algorithm for the pressure calculations.

2.3 Boundary Conditions

The current numerical simulation in this project aimed to investigate the Nusselt number and the flow phenomena at the sudden expansion in annular pipe. The diagram of the concentric pipe was drawn and meshed by using Gambit software generating 11,000 cells, in which the result was validated with the findings from Al-aswadi *et al.* [14]. As the geometry of the annular pipe is symmetrical, only the lower half was drawn and simulated. Finite volume-based CFD solver FLUENT 6.3 was used for this investigation. The iteration

of the standard K-epsilon viscous model is based on energy and Reynolds averaged Navier–Stokes equations. The viscous model also provides good solutions for steady, near wall treatment, axisymmetric, incompressible and turbulent flow. The first-order upwind scheme was used to solve the field variables while steady assumption was selected for all the cases where convergence can be obtained. Simulations were performed until the residual values were less than 1×10^{-4} for such convergence purpose. Five different Reynolds numbers were tested in the simulation, Re = 5000, 10000, 15000 and 20000 and 25000 to produce fully developed turbulent steady nanofluid flow, where the heat flux applied to the inner tubes were varied from q = 719 W/m^2 to 2098 W/m^2. Pressure-based solver with second-order implicit steady formulation, with standard k-epsilon equation [20], was applied in defining the model. Second-order upwind scheme is applied in solving the momentum, turbulent kinetic energy and turbulent dissipation rate and energy discretizations [21]. The boundary condition of the inlet is defined as velocity inlet, whereas for outlet it is pressure outlet with turbulent intensity of 7% and turbulent length scale 0.02 m. The Reynolds number (Re_d) can be obtained by the following Equation (7):

$$Re_d = \frac{\rho U D_h}{\mu} \tag{7}$$

where ρ is the density of the fluid, U is the velocity of the fluid, D_h the hydraulic diameter of the annular pipe and μ is the dynamic viscosity of the fluid. The local heat transfer coefficient is calculated using convection heat flux as shown by Equation (8):

$$h_x = \frac{q_c}{(T_{sx} - T_{bx})} \tag{8}$$

where q_c is the convection heat flux, T_{sx} is the local surface temperature *and* T_{bx} is the local bulk fluid temperature. The local Nusselt number (Nu) can be evaluated by Equation (9):

$$Nu = \frac{h_x d}{k} \tag{9}$$

where d is the diameter of the pipe and K is the thermal conductivity.

2.4 Code Validation

The process of numerical validation method consists of running the numerical code under specific conditions for selected benchmark [14] and then comparing the results with the experimental or theoretical numerical data in the literature.

The case simulated for validation purpose was the forced convective nanofluids flow over a horizontal backward facing step placed in a duct [14]. For this validation the Reynolds numbers chosen are in the laminar regime (Re = 50 and 175). Figure 2 to 4 show the results of the comparison with Al-aswadi *et al.* [14] for different nanofluids.

The velocity distributions for various X/s in the recirculation region along the duct are shown in Figures 2 to 3. The recirculation region clearly appears and the size of the recirculation region decreases as the distance between the step and the stepped wall increases until the flow reaches the reattachment point where the flow exhibits almost zero velocity, as shown in Figures 2 (a - d) and 3 (a - d). Figure 2 (a - c) and Figure 3 (a - c) show that there is a recirculation region developed downstream of the step. Downstream of this point the flow starts to become fully developed flow as the fluid flows towards the duct exit as shown in Figures 2(d) and 3(d).
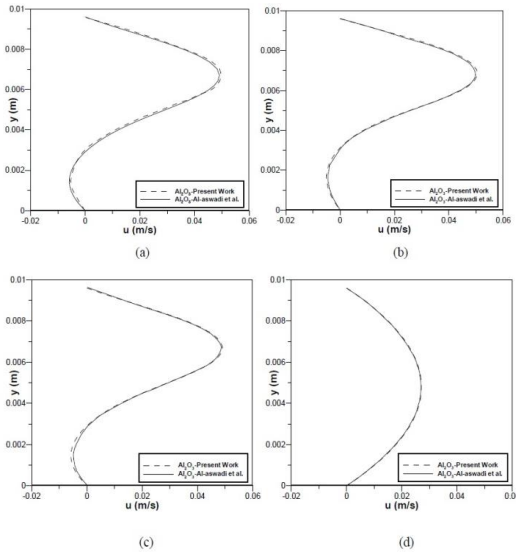

Figure 2 Comparison of velocity distribution with the results of Al-aswadi *et al*. [14] in the recirculation region for S = 4.8 mm, and ER = 2 at Re =175 for Al₂O₃ at different X/s, (a) 1.04, (b) 1.92, (c) 2.6, (d) 32.8
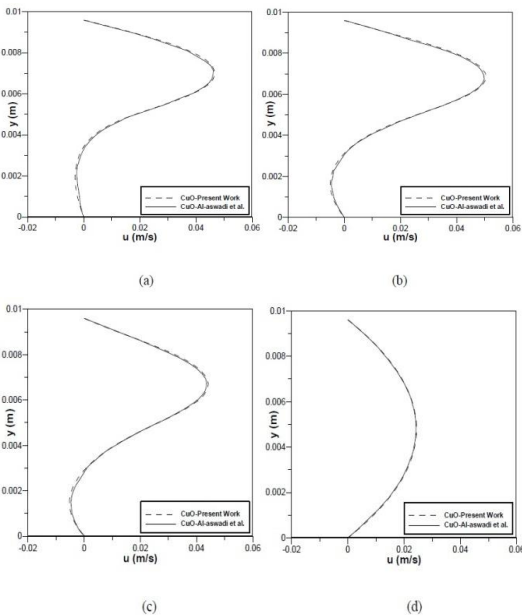
Figure 3 Comparison of velocity distribution with the results of Al-aswadi *et al*. [14] in the recirculation region for S = 4.8 mm, and ER = 2 at Re =175 for CuO at different X/s, (a) 1.04, (b) 1.92, (c) 2.6, (d) 32.8

Figure 4 shows the skin friction coefficient at the bottom wall downstream of the step. The skin friction coefficient initially increases abruptly as the distance downstream from the step increases. It then decreases monotonically until it reaches its minimum peak. Then the minimum peak formed a shattering fluctuation. Anyhow it keeps increasing in a general trend, until it reaches a point where the skin friction coefficient remains constant along the rest of the bottom wall. This shows that the skin friction coefficient is approaching asymptotically the fully developed channel flow.
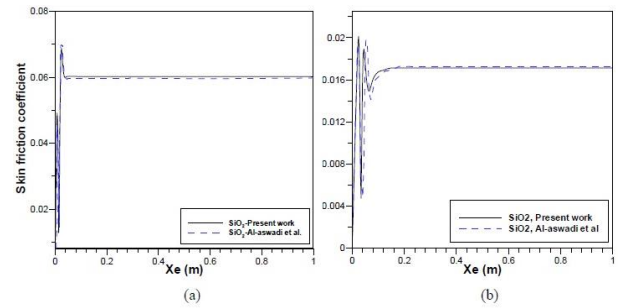
Figure 4 Nanofluids for Different Reynolds Numbers (a) Re = 50 and (b) Re = 175 at the Bottom Wall Downstream the Step

2.5 Thermal Physical Properties of Nanofluids

In order to carry out simulations for nanofluids, the effective thermophysical properties of nanofluids must be calculated first. In this case, the nanoparticle being used is SiO_2. Basically the required properties for the simulations are effective thermal conductivity (k_{eff}), effective dynamic viscosity (μ_{eff}), effective mass density (ρ_{eff}), effective coefficient of thermal expansion (β_{eff}) and effective specific heat capacity (Cp_{eff}).

The effective properties of mass density, specific heat and coefficient of thermal expansion are actually calculated according to the mixing theory.

By using Brownian motion of nanoparticles in backward facing step having a baffle, the effective thermal conductivity can be obtained following mean empirical correlation [22]:

$$k_{eff} = k_{Static} + k_{Brownian} \tag{10}$$

Static Thermal Conductivity:

$$k_{Static} = k_{bf}\left[\frac{k_{np}+2k_{bf}-2(k_{bf}-k_{np})\emptyset}{k_{np}+2k_{bf}+(k_{bf}-k_{np})\emptyset}\right] \tag{11}$$

Brownian Thermal Conductivity:

$$k_{Brownian} = 5\text{x}10^4\beta\emptyset\rho_{bf}c_{p,bf}\sqrt{\frac{\kappa T}{2\rho_{np}R_{np}}}.f(T,\emptyset) \tag{12}$$

where Boltzmann constant:

$$k = 1.3807\text{x}10^{-23}\text{J/K}$$

while the rest of the value of K can be referred in Table 2 which manifested the thermophysical properties of pure water and various types of nanofluids modeling function, β [23]:

$$\beta = 0.0137(100\emptyset)^{-0.8229} \text{for} \emptyset < 1\%$$
$$\beta = 0.0011(100\emptyset)^{-0.7272} \text{for} \emptyset > 1\%$$

Modeling function,

$$f(T, \emptyset) = (2.8217x10^{-2}\emptyset) + 3.917x10^{-3}\left(\frac{T}{T_0}\right)$$
$$+ (-3.0699x10^{-2}\emptyset - 3.91123x10^{-3})$$

Table 2 Thermophysical properties of pure water and various types of nanofluids

Thermophysical Properties	Water	Al2O3	CuO	ZnO	SiO2
Density, ρ(kg/m³)	998.203	3970	6500	5600	2200
Dynamic Viscosity, μ(Ns/m²)	2.01×10^{-3}	-	-	-	-
Thermal Conductivity, k (W/m.K)	0.613	40	20	13	1.2
Specific Heat, cp (J/kg.K)	4182.2	765	535.6	495.2	703
Coefficient of Thermal Expansion, β (1/K)	2.06×10^{-4}	5.8×10^{-6}	4.3×10^{-6}	4.3×10^{-6}	5.5×10^{-6}

By using Brownian motion of nanoparticles the effective viscosity can be obtained by using the following empirical correlation [24]:

Viscosity:

$$\frac{\mu_{eff}}{\mu_f} = \frac{1}{1 - 34.87\left(\frac{d_p}{d_f}\right)^{-0.3} \emptyset^{1.03}} \tag{13}$$

Equivalent diameter of base fluid molecule:

$$d_f = \left[\frac{6M}{N\pi\rho_{bf}}\right]^{1/3} \tag{14}$$

The density of the nanofluidρ_{nf} can be calculated using [22]:

$$\rho_{nf} = (1 - \emptyset)\rho_f + \emptyset\rho_{np} \tag{15}$$

Whereby ρ_f and ρ_{np} are the mass densities of the base fluid and the solid nanoparticles, respectively.

The effective heat capacity at constant pressure of the nanofluid$(\rho c_p)_{nf}$ can be calculated using [22]:

$$(\rho c_p)_{nf} = (1 - \emptyset)(\rho c_p)_f + \emptyset(\rho c_p)_{np} \tag{16}$$

as $(c_p)_f$ and$(c_p)_{np}$are the effective heat capacities of base fluid and nanoparticles, respectively.

The effective coefficient of thermal expansion of nanofluid $(\rho\beta)_{nf}$ can be calculated using [22]:

$$(\rho\beta)_{nf} = (1 - \emptyset)(\rho\beta)_f + \emptyset(\rho\beta)_{np} \tag{17}$$

as $(\beta)_f$ and $(\beta)_{np}$ are thermal expansion coefficients of base fluid and nanoparticles, respectively.

3.0 RESULTS AND DISCUSSIONS

3.1 The Effect of Nanofluids Parameters

Different type of nanoparticles which are Al₂O₃, CuO, SiO₂ and ZnO and pure water as the base fluid were used. In order to see the effects of different nanofluids on the heat transfer enhancement all other parameters were fixed, $\varphi = 0.04$, and $d_p = 25$ nm, at Re = 5000, q = 719 W/m² and a step height equal to 18.5 nm, i.e. (d/D = 1.8) along the downstream wall. Figure 5 shows the variations of the surface temperature along the heated wall. All the nanofluids demonstrated similar trend that the temperature increases steadily along the downstream of flow.
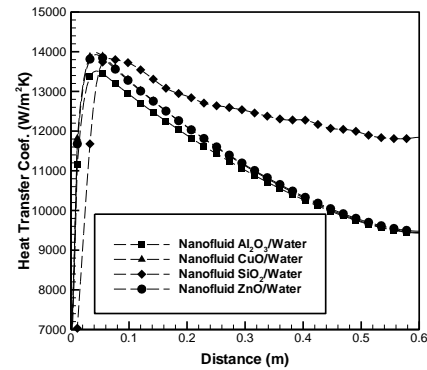
Figure 5 Surface temperatures distributions for different nanofluids with φ= 4%, d_p =25 nm for Re = 5000, d/D = 1.8 and q = 517 W/m².

The local heat transfer coefficient keeps decreasing along the heated wall after an abrupt rise at the proximity of the entrance, as shown in Figure 6. This is due to the temperature difference when the reversed
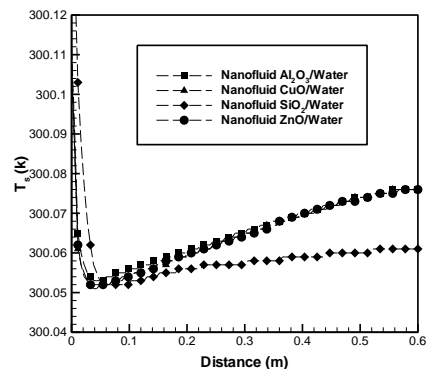
Figure 6 Heat transfer distributions for different nanofluids with φ = 4%, d_p =25 nm for Re = 5000, d/D = 1.8 and q = 517 W/m²

flow attached with the main separated flow which has a lower temperature. It is found in this figure that the base fluid with SiO_2 nanofluid has the highest maximum peak in Nusselt number followed by Al_2O_3, CuO, and ZnO. This is because inside the recirculation zone the nanofluid exhibited lower density and thermal conductivity.

3.2   The Effect of Different Heat Fluxes

Figure 7 shows the variation of the surface temperature along the heated wall for different heat fluxes with a specific SiO_2, φ= 4%, dp =25 nm, Re = 5000 and a step height equal to (18.5), i.e. (d/D = 1.8). The general shape shows a reduction of surface temperature at the test section inlet directly behind the step. The minimum magnitude of temperature was obtained at a specific axial position where the flow reattachment took place after the separation region due to turbulence augmented heat transfer. Then the temperature gradually increased to reach a maximum value, with decreasing heat transfer coefficient approaching the test tube exit under the influence of end loss. From Figure 8, it can be seen that the effect of different heat fluxes on the distributions of heat transfer coefficient was insignificant. It is inferred that the imposition of the experimented heat flux will not trigger the change of internal composition of nanofluids, which in return will possibly influence their heat transfer coefficients.
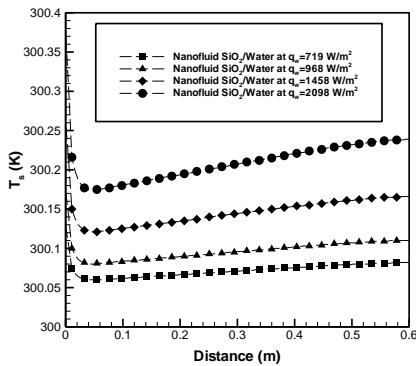

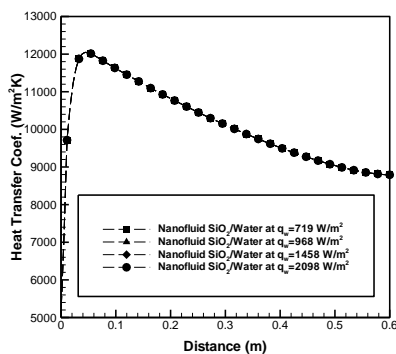**Figure 7** Surface temperatures distributions for different heat wall fluxes with SiO_2, φ= 4%, d_P =25 nmfor Re = 5000, d/D = 1.8.

Figure 8 Heat transfer coefficient distributions for different heat wall fluxes withSiO_2, φ= 4%, d_P =25 nm for Re = 5000, d/D = 1.8.

3.3   The Effect of Different Reynolds Number

The effect of variation of Reynolds numbers on the outer surface wall temperature and the surface of heat transfer coefficient) is shown in Figures 9 and 10 respectively, with the similar condition in which the nanoparticle is SiO_2, φ= 4%, dp =25 nm, q = 719 W/m^2 and s = (18.5), i.e. d/D = 1.8. Figure 9 shows that the surface temperature variation decreases as the Reynolds number increases for the same heat flux and step height. Generally the temperature change is insignificant, and this further indicates the stability of thermal characteristics of nanofluids. The results also show the increment of surface temperature along the pipe. The maximum temperature was obtained at zero distance. The temperature profile shows a sharp drop with a gradually increment along the pipe. The distribution of the local heat transfer coefficient at (18.6) step height and the constant heat flux of q = 719 W/m^2 for different Reynolds numbers are plotted in Figure 10. It shows the effect of the different Reynolds number on the heat transfer coefficient. This is in accordance with the increasing trend of temperature along the downstream field as illustrated in Figure 9.
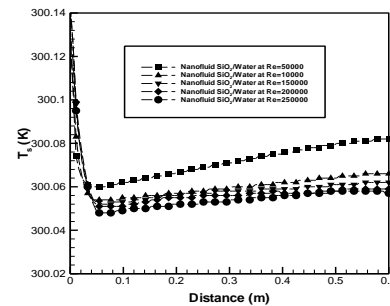

Figure 9 Surface temperatures distributions for different Reynolds numbers with SiO_2, φ= 4%, d_P =25 nm for q=517 W/m^2, d/D = 1.8.

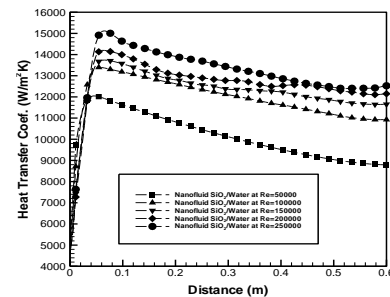**Figure 10** Heat transfer coefficient distributions for different Reynolds numbers with SiO_2, φ= 4%, d_P =25 nm for q=517 W/m^2, d/D = 1.8.

3.4   The Effect of Different Step Heights

In Figure 11, the results represent increase of Nusselt number following the presence of the step heights. By increasing the Reynolds number, higher value of average Nusselt number was obtained. Also, the presence of backward-facing step induces turbulent

flow and hence increases the average Nusselt number.
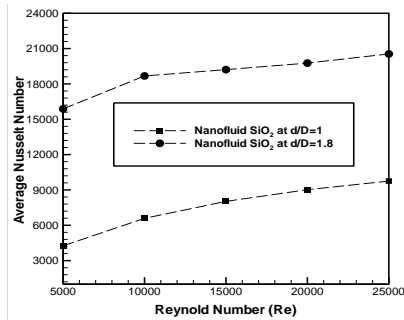
Figure 11 Average Nusselt Number distributions for different step heights with SiO_2, φ= 4%, d_p =25 nm for q=517 W/m^2, d/D = 1.8

4.0 CONCLUSION

Numerical simulation of turbulent mixed convection heat transfer of nanofluids flow over an annular passage was carried out. The emphasis is given on the heat transfer enhancement resulting from various parameters, which include the different type of nanofluids, different Reynolds numbers, different heat wall fluxes and different step heights. The governing equations were solved utilizing finite volume method with the SIMPLE algorithm. The following conclusions can be drawn from this study:

1. In step annular flow surface temperature in the separation zone shows a notable reduction in magnitude for the same Re and heat flux and the reduction magnitude increases with the increase of step height.
2. Increase of inlet flow velocity and step height will reduce the surface temperature to a lowest temperature, and then increase along the test section. This lowest temperature occurs at the flow reattachment point.
3. The local heat transfer coefficient (h_x) increases as the Reynolds number increases for all cases with or without step. In the separation region (recirculation zone) the local heat transfer coefficient keeps increasing until it reaches a maximum value at the reattachment point.
4. With the increase of Reynolds number, the reattachment point moves toward downstream from the step. The location of maximum heat transfer (reattachment point) is presumed to be at the end of the separated flow region, moves downstream as the step height increases.

Acknowledgement

Nomenclature

Roman Symbols

u	Horizontal velocity, mm/s
v	Vertical velocity, mm/s
x	Horizontal distance, mm
y	Vertical distance, mm
T	Temperature, K
d	Inner diameter of outer tube, mm
D_h	Hydraulic diameter of inner tube, mm
D_i	Outer diameter of annular passage, mm
K	Thermal conductivity, W/m.K
Re_d	Reynolds number at hydraulic diameter
Al_2O_3	Aluminum Oxide
C_p	Specific heat, KJ/kg.K
d_p	Diameter of nanofluid particles, nm
K	Thermal conductivity, W/m.K
SiO_2	Silicon Oxide
d_h	Hydraulic diameter of outer tube, mm
D	Inner diameter of inner tube, mm
h	Heat transfer coefficient, W/m^2.K
L	Length of the annular passage, mm
Nu_d	Nusselt number at hydraulic diameter
CFD	Computational Fluid Dynamic
CuO	Copper Oxide
ER	Expansion ratio = H/(H-S)
q	Wall heat flux, W/m^2
ZnO	Zinc Oxide
s	Step height
X	Downstream length, mm

Greek Symbols

ε	Turbulent dissipation rate, m^2/s^2
a	Thermal diffusivity of the fluid, m^2/s
μ_k	Turbulent viscosity
ρ	Density, kg/m^3
β	Volumetric coefficient of thermal expansion, 1/K
μ	Dynamic viscosity, N.m/s
υ	Kinematic viscosity, m^2/s
φ	Nanoparticles volume fraction (%)

Subscripts

bf	Base fluid
nf	Nanofluid
s	Solid
f	Fluid
p	Particles

References

[1] Tihon, J., Pěnkavová, V., Havlica, J. and Šimčík, M. 2012. The Transitional Backward-facing Step Flow in A Water Channel with Variable Expansion Geometry. *Experimental Thermal and Fluid Science*. 40: 112-125.

[2] Östlund, J. 2004. *Supersonic Flow Separation with Application to Rocket Engine Nozzles*. Technical Reports, Department of Mechanics, Royal Institute of Technology, Stockholm, Sweden.

[3] De La Calzada, P., Valdes, M. and Burgos, M.A. 2011. Heat transfer in separated flows on the pressure side of turbine blades. *Numerical Heat Transfer, Part A: Applications*. 60(8): 666-684.

[4] Togun, H., Salman, Y.K., Sultan Aljibori, H.S., and Kazi, S.N. 2011. An Experimental Study of Heat Transfer to Turbulent Separation Fluid Flow in An Annular Passage. *International Journal of Heat and Mass Transfer*. 54: 766-773.

[5]   Wang, B., Zhang, H.Q. and Wang, X.L. 2008. A Time-series Stochastic Separated Flow (TSSSF) Model for Turbulent Two-phase Flows. *Numerical Heat Transfer, Part B: Fundamentals*. 55: 73-90.

[6]   Terekhov, V.I. and Pakhomov, M.A. 2009 Predictions of Turbulent Flow and Heat Transfer in Gas-Droplets Flow Downstream of a Sudden Pipe Expansion. *International Journal of Heat and Mass Transfer*. 52: 4711-4721.

[7]   Kurtbaş, I. 2008. The Effect of Different Inlet Conditions of Air in a Rectangular Channel on Convection Heat Transfer: Turbulence Flow. *Experimental Thermal and Fluid Science*. 33: 140-152.

[8]   Kays, W.M. and Leung, E.Y. 1963. Heat Transfer in Annular Passage – Hydrodynamically Developed Turbulent flow with Arbitrarily Prescribed Heat Flux. *Journal of Heat and Mass Transfer*. 6: 537–557.

[9]   Barbosa S., J.G., Anand, N.K. and Sarin, V. 2005. Forced Convection over A Three-dimensional Horizontal Backward-facing Step. *International Journal of Computational Engineering Science*. 6: 225–234.

[10] Filletti, E.G. and Kays, W.M. 1967. Heat Transfer in Separated Reattached and Redevelopment Regions Behind a Double Step at Entrance to a Flat Duct. *Journal of Heat transfer, ASME*. 89: 163–168.

[11] Davletshin, A., Mikheev, N.I. and Molochnikov, V.M. 2008. Heat Transfer in a Turbulent Separation Region with Superimposed Stream Pulsations. *Journal of Thermo Physics and Aeromechanics*. 15: 215–222.

[12] Sparraw, E.M., Abraham, J.P. and Minkowycz, W.J. 2009. Flow Separation in A Diverging Conical Duct: Effect of Reynolds Number and Divergence Angle. *International Journal of Heat and Mass Transfer*. 52: 3079–3083.

[13] Murata, A. and Iwamoto, K. 2011. Heat and Fluid Flow in Cylindrical and Conical Annular Flow-Passages with Through Flow and Inner Wall Rotation. *International Journal of Heat and Fluid Flow*. 32: 378–391.

[14] Al-aswadi, A.A., Mohammed, H.A. Shuaib, N.H. and Campo, A. 2010. Laminar Forced Convection Flow over a Backward-facing Step using Nanofluids. *International Communications in Heat and Mass Transfer*. 37: 950–957.

[15] Roslan, R., Saleh, H. and Hashim, I. 2011. Buoyancy-driven Heat Transfer in Nanofluid-Filled Trapezoidal Enclosure with Variable Thermal Conductivity and Viscosity. *Numerical Heat Transfer, Part A: Applications*. 60: 867–882.

[16] Raisi, A., Ghasemi, B. and Aminossadati, S.M. 2011. A Numerical Study on The Forced Convection of Laminar Nanofluid in A Microchannel with Both Slip and No-slip Conditions. *Numerical Heat Transfer, Part A: Applications*. 59: 114–129.

[17] Ghasemi, B. and Aminossadati S.M. 2009. Natural Convection Heat Transfer in An Inclined Enclosure Filled with A Water-CuO Nanofluid. *Numerical Heat Transfer, Part A: Applications*. 55: 807–823.

[18] Zhang, Y., Li, L., Ma, H.B. and Yang, M. 2009. Effect of Brownian and Thermophoretic Diffusions of Nanoparticles on No Equilibrium Heat Conduction in A Nanofluid Layer with Periodic Heat Flux. *Numerical Heat Transfer, Part A: Applications*. 56: 325–341.

[19] Chen, Y.T., Nie, J.H., Hsieh, H.T. and Sun, L.J. 2006. Three-dimensional Convection Flow Adjacent to Inclined Backward-facing Step. *International Journal of Heat and Mass Transfer*. 49: 4795–4803.

[20] Yakhot, V., Orszag, S.A., Thangam, S., Gatski, T.B. and Speziale, C.G. 1992. Development of Turbulence Models for Shear Flows by A Double Expansion Technique. *Physics of Fluids*. 4: 1510–1520.

[21] Lee, D.H., Lee, J.S., Park, H.J. and Kim, M.K. 2011. Experimental and Numerical Study of Heat Transfer Downstream of an Axisymmetric Abrupt Expansion and in a Cavity of a Circular Tube. *Journal of Mechanical Science and Technology*. 25: 395–401.

[22] Ghasemi, B. and Aminossadati, S.M. 2010. Brownian Motion of Nanoparticles in a Triangular Enclosure with Natural Convection. *International Journal of Thermal Sciences*. 49: 931-940.

[23] Vajjha, R.S. and Das, D.K. 2009. Experimental Determination of Thermal Conductivity of Three Nanofluids and Development of New Correlations. *International Journal of Heat and Mass Transfer*. 52: 4675-4682.

[24] Tiwari, R.K. and Das, M.K. 2007. Heat Transfer Augmentation in a Two-sided Lid-driven Differentially Heated Square Cavity utilizing Nanofluids. *International Journal of Heat and Mass Transfer*. 50: 2002-2018.